Exploring the spatio-temporal dynamics of an optically pumped semiconductor laser with intracavity second harmonic generation

Hsing-Chih Liang, Yi-Chun Lee, Jung-Chen Tung, Kuan-Wei Su, Kai-Feng Huang, and Yung-Fu Chen*

Department of Electrophysics, National Chiao Tung University, Hsinchu 30010, Taiwan
**Corresponding author: yfchen@cc.nctu.edu.tw*

Received August 8, 2012; revised September 21, 2012; accepted September 28, 2012;
posted September 28, 2012 (Doc. ID 174049); published November 6, 2012

We experimentally observe an intriguing phenomenon of complex spatio-temporal dynamics in a commercial optically pumped semiconductor laser with intracavity second harmonic generation. We numerically verify that the experimental results come from the total mode locking of transverse electromagnetic modes (TEM_{00}) and higher-order modes with significant astigmatism. The scenarios of the spatio-temporal dynamics are quite similar to the phenomena in soft-aperture Kerr-lens mode locked Ti:sapphire lasers. © 2012 Optical Society of America

OCIS codes: 140.7270, 140.4050, 190.3270.

Since the first demonstration of self-mode locking in the Ti-sapphire laser by Spence *et al.* [1], the phenomena of Kerr-lens mode locking (KLM) has been widely explored both experimentally and theoretically [2–6]. Recently, KLM experiments have been demonstrated for the Yb-doped [7–10] and Nd-doped [11–13] solid-state lasers. More recently, the self-mode-locked operation with a linear cavity has also been observed in the optically pumped semiconductor laser (OPSL) [14]. The OPSL, with intracavity second harmonic generation (SHG), has become a technologically promising and commercially developed light source [15]. In spite of the wide-spread commercial and academic usage, the issue of whether the phenomenon of self-mode locking prevails in conventional OPSLs with intracavity SHG has not been verified.

In this Letter we experimentally explore the dynamics of a commercial OPSL with intracavity SHG for 532 nm emission. Experimental measurements reveal that the laser beam displays a phenomenon of complex spatio-temporal dynamics in the scale of the round-trip time. We employ the cavity configuration to calculate the tangential and sagittal mode sizes and frequency spacings of longitudinal and transverse modes for investigating the origin of the spatio-temporal dynamics. With the calculated parameters and the numerical fitting, we verify that the experimental observation can be explained in terms of the total mode locking [16,17] of transverse electromagnetic modes (TEM_{00}) and few high-order modes with significant astigmatism. The verification indicates that self-mode locking inherently prevails in conventional OPSLs. Therefore, it can be expected that the OPSLs can be straightforwardly employed to generate ultrafast light pulses through self-mode locking. More importantly, the operation wavelength can be tailored by band gap engineering.

In our experiments, we employed the OPSL-532platform, a commercially available OPSL from Coherent Inc., emitting 5 W of average power at 532 nm. Figure 1 is a schematic diagram of this laser. The configuration is an intracavity doubled "V-cavity" with the semiconductor gain chip and a birefringent filter (BRF) on the first arm and the doubling LBO crystal on the second arm. The BRF is used to set the output wavelength. The physical lengths are approximately 64 mm and 42 mm for the first and second arms, respectively. The angle θ between two cavity arms is approximately 17.5°. A flat mirror next to the crystal has high reflectivity (HR) coatings for both the fundamental and second harmonic, the curved output coupler (OC) is coated to reflect the fundamental harmonic and transmit the second harmonic. The radius of curvature R of the OC is 75 mm. In this configuration, the emission in the 532 nm regime can be achieved with a double pass doubling in the LBO crystal and emitted on a single output. The whole laser cavity, together with the semiconductor gain chip on a heat sink, is cooled with thermoelectric coolers. The semiconductor gain media is a multiple quantum well structure that is optically pumped sidewise. More detailed discussion of the high power OPSLs emitting in blue and green could be found elsewhere [18].

Figure 2(a) shows the power versus current curve for the green OPSL system. The threshold current for lasing is found to be approximately 11 A. The laser module can produce 5.5 W at the rated current of 28 A. The temporal dynamics was detected by a high-speed InGaAs photodetector (Electro-optics Technology Inc. ET-3500 with rise time of 35 ps), whose output signal was connected to a digital oscilloscope (Agilent DSO 80000) with a 10 GHz electrical bandwidth and a sampling interval of 25 ps. A Fourier optical spectrum analyzer (Advantest Q8347), which is constructed with a Michelson interferometer, was employed to monitor the spectral information with a resolution of 0.002 nm. Figure 2(b) shows the spectral

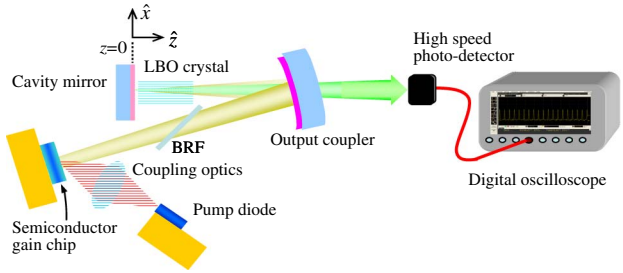

Fig. 1. (Color online) Cavity configuration of the OPSL system.

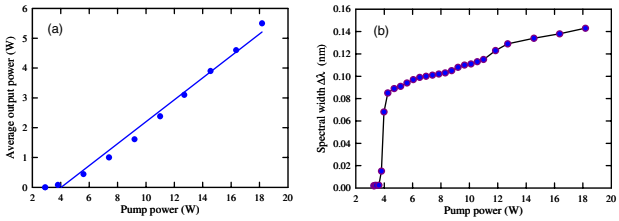

Fig. 2. (Color online) (a) Output power versus current curve for the OPSL system. (b) FWHM spectral width versus the pump current.

width at half the line maximum (FWHM) versus the pump current for the green OPSL system. For the pump current slightly above the threshold in the range of 11.0–11.7 A, the lasing spectral reveals the system to be in the single-longitudinal-mode operation. Consistently, we also found that there were no obvious oscillations in the real-time trace in the GHz domain for the pump current within 11.0–11.7 A. On the other hand, the spectral width abruptly increases for the pump current above 11.8 A and stars to slowly increase for the pump current greater than 12.5 A. The laser system can be confirmed to be in the multi-longitudinal-mode operation. The spectral width indicated that the number of the longitudinal modes was approximately 30 at maximum output. The beam profile was measured with a CCD camera with an adjustable attenuator. Figure 3(a) depicts the mode pattern at a distance of 300 mm from the OC. The laser mode exhibits an elliptical pattern that originates in the astigmatism of the V-cavity. The astigmatism comes from the fact that the effective radius of curvature of the OC in Fig. 1, due to the title angle, should be $R/\cos\,\theta$ and $R/\cos\,\theta$ for the tangential and sagittal planes, respectively. The three marked locations in Fig. 3(a) are the positions where the temporal traces are measured for exploring the dynamics.

Figures 4(a)–4(c) show typical results of the temporal traces obtained at the pump current of 12.0 A for three positions corresponding to labels 1–3 shown in Fig. 3(a), respectively. The coordinates with the unit in mm for the labels 1–3 are $(x, y, z) = (0, 2, 300)$, $(0, 0, 300)$, and $(1.5, 0, 300)$, respectively. It can be seen that the time trace displays a phenomenon of spatio-temporal dynamics. The observed phenomenon implies that the laser output is not in single transverse mode. We measured the beam quality factor M^2 and found it to be approximately 1.3. This result indicates that the lasing mode is mainly contributed by $\mathrm{TEM}_{0,0}$ and few high-order $\mathrm{TEM}_{n,m}$ modes. In the following, we verify that the spatio-temporal dynamics can be explained in terms of total mode locking [16,17] of $\mathrm{TEM}_{0,0}$ and some astigmatic high-order modes.

As shown in Fig. 1, the horizontal and vertical directions correspond to the x- and y-axes, respectively and

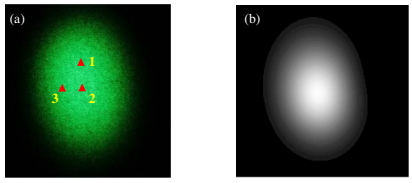

Fig. 3. (Color online) (a) Experimental mode pattern at a distance of 300 mm from the OC. (b) Numerical mode pattern.

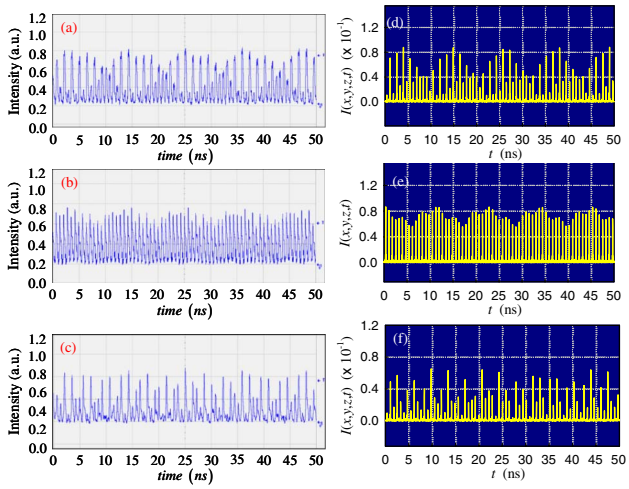

Fig. 4. (Color online) (a)–(c) Typical results of the temporal traces obtained at the pump current of 12.0 A for three positions corresponding to the labels 1–3 shown in Fig. 3(a), respectively. (d)–(f) Numerically reconstructed pulse trains.

the output beam propagates along the z direction with $z = 0$ at the cavity flat mirror. With these coordinates, the output beams of the V-cavity can be expressed as astigmatic Hermite–Gaussian modes [19]:

$$\Phi_{n,m,l}(x, y, z, t) = \psi_{n,m}^{(\mathrm{HG})}(x, y, z, t)e^{-il\Omega_z t_z} \tag{1}$$

with

$$\psi_{n,m}^{(\mathrm{HG})}(x, y, z, t) = \frac{\sqrt{2}}{\sqrt{\omega_x(z)\omega_y(z)}}\psi_n(\tilde{x}, \phi_x)\psi_m(\tilde{y}, \phi_y), \tag{2}$$

$$\psi_n(\xi, \vartheta) = \left(2^n n! \cdot \sqrt{\pi}\right)^{-1/2} e^{-\xi^2/2} H_n(\xi) e^{-i(n+1/2)\vartheta}, \tag{3}$$

and

$$t_z = t - \frac{z}{c}\left[1 + \frac{x^2}{2(z^2 + z_{Rx}^2)} + \frac{y^2}{2(z^2 + z_{Ry}^2)}\right], \tag{4}$$

where $\tilde{x} = \sqrt{2}x/\omega_x(z)$, $\tilde{y} = \sqrt{2}y/\omega_y(z)$, $\omega_x(z) = \omega_{ox}\sqrt{1 + (z/z_{Rx})^2}$, $\omega_y(z) = \omega_{oy}\sqrt{1 + (z/z_{Ry})^2}$, $z_{Rx} = \pi\omega_{ox}^2/\lambda$, $z_{Ry} = \pi\omega_{oy}^2/\lambda$, $\phi_y = \Omega_y t_z + \theta_y(z)$, $\phi_x = \Omega_x t_z + \theta_x(z)$, $\theta_x(z) = \tan^{-1}(z/z_{Rx})$, $\theta_y(z) = \tan^{-1}(z/z_{Ry})$, where ω_{ox} and ω_{oy} are the horizontal and vertical radii of the beam on the cavity mirror, λ is the emission wavelength, Ω_z is the longitudinal mode spacing, Ω_x and Ω_y are the horizontal and vertical mode spacings, l is the longitudinal mode index, and n and m are the transverse mode indices. With the ABCD matrix formalism [19] and the cavity parameters, ω_{ox} and ω_{oy} can be numerically calculated to be approximately 47.9 μm and 33.7 μm, respectively. The longitudinal frequency spacing $\Omega_z/2\pi$ is found to be approximately 1.378 GHz. With the same analysis, Ω_x and Ω_y can be found to be approximately 0.403 Ω_z and 0.467 Ω_z.

Considering the laser beam that consists of a single transverse mode and N longitudinal modes with equal amplitude and phase locking, the normalized electric field can be given by

$$\Psi_{n,m,N}(x,y,z,t) = \frac{1}{\sqrt{N}} \sum_{l=l_o}^{l_o+N} \Phi_{n,m,l}(x,y,z,t), \qquad (5)$$

where $N+1$ is the number of longitudinal modes and l_o is the lowest index of the longitudinal modes. Based on a thoroughly numerical fitting, we find that the typical spatio-temporal behavior of Fig. 4 can be interpreted as the simultaneous coherent locking of five transverse modes $\Psi_{n,m,N}(x,y,z,t)$ with several tens of longitudinal modes. We employ the numerical analysis to obtain a compact expression for describing the experimental laser wave:

$$E(x,y,z,t) = \sum_{s=0}^{2} a_s[\Psi_{s,0,N}(x,y,z,t) + \Psi_{0,s,N}(x,y,z,t)], \qquad (6)$$

where the coefficient a_s represent the relative amplitudes of the transverse modes with different orders. With Eq. (6), for the best fit to the experimental data, we find that the results shown in Figs. 4(a)–4(c) can be excellently reconstructed with the coefficient a_s to be $a_0 = 0.5$, $a_1 = 0.3$, and $a_2 = 0.1$. Figures 4(d)–4(f) show the numerical pulse trains with the coordinates corresponding to the experimental positions shown in Figs. 4(a)–4(c), respectively. It can be seen that the numerical results agree very well with the experimental data. More specifically, the period of the pulse train in Fig. 3(b) comes from the coherent interference of longitudinal modes, whereas the beating of the transverse modes cause the additional envelops in Figs. 3(a) and 3(b). The difference of the beating envelops arises from the considerable astigmatism of the V-cavity. Furthermore, the numerical transverse pattern shown in Fig. 3(b) is consistent with the experimental measurement shown in Fig. 3(a). The good agreement confirms that the spatio-temporal dynamics of the output beam arises from the total mode locking [16,17] of TEM_{00} and higher-order modes with significant astigmatism.

The autocorrelation traces were also performed with a commercial autocorrelator (APE pulse check, Angewandte physic & Elektronik GmbH). Figure 5(a) shows the FWHM of the pulse duration in the autocorrelation trace for the central position as a function of the pump current, where the temporal intensity is assumed to be a sech^2 profile. A typical autocorrelation trace obtained at a pump current of 16 A is shown in the inset of Fig. 5(b). The pulse duration can be down to approximately 2.1 ps at an output power of 5.5 W. With the optical spectra shown in Fig. 2(b), the overall time-bandwidth product of the mode-locked pulse can be found to be 0.32, which is quite close to the Fourier-limited value.

In conclusion, we have experimentally explored the spatio-temporal dynamics in the scale of the round-trip time in an OPSL system with intracavity SHG. We have numerically confirmed that the spatio-temporal dynamics can be reconstructed with the total mode locking of TEM_{00} and astigmatic higher-order modes. The time-bandwidth product of the mode-locked pulse is very close to the Fourier-limited value for all output powers. Since the cavity astigmatism can be eliminated or reduced by the appropriate design, it is believed that the OPSLs can be directly exploited to generate ultrafast light pulses with wavelength versatility through self-mode locking and band gap engineering.

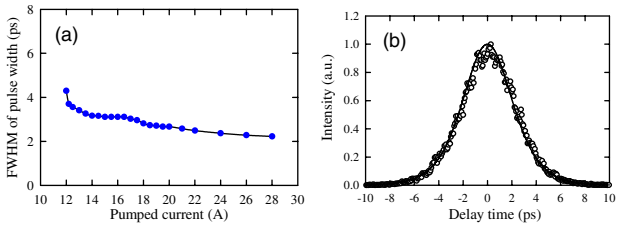

Fig. 5. (Color online) (a) FWHM of the pulse duration in the autocorrelation trace for the central position as a function of the pump current. (b) Typical autocorrelation trace obtained at a pump current of 16 A.

The authors acknowledge the National Science Council of Taiwan for their financial support of this research under contract NSC 100-2628-M-009-001-MY3.

References

1. D. E. Spence, P. N. Kean, and W. Sibbett, Opt. Lett. **16**, 42 (1991).
2. J. L. A. Chilla and O. E. Martinez, J. Opt. Soc. Am. B **10**, 638 (1993).
3. G. Cerullo, S. De Silvestri, V. Magni, and L. Pallaro, Opt. Lett. **19**, 807 (1994).
4. D. Cote and H. M. van Driel, Opt. Lett. **23**, 715 (1998).
5. S. R. Bolton, R. A. Jenks, C. N. Elkinton, and G. Sucha, J. Opt. Soc. Am. B **16**, 339 (1999).
6. J.-H. Lin, M.-D. Wei, W.-F. Hsieh, and H.-H. Wu, J. Opt. Soc. Am. B **18**, 1069 (2001).
7. H. Liu, J. Nees, and G. Mourou, Opt. Lett. **26**, 1723 (2001).
8. A. A. Lagatsky, A. R. Sarmani, C. T. A. Brown, W. Sibbett, V. E. Kisel, A. G. Selivanov, I. A. Denisov, A. E. Troshin, K. V. Yumashev, N. V. Kuleshov, V. N. Matrosov, T. A. Matrosova, and M. I. Kupchenko, Opt. Lett. **30**, 3234 (2005).
9. G. Q. Xie, D. Y. Tang, L. M. Zhao, L. J. Qian, and K. Ueda, Opt. Lett. **32**, 2741 (2007).
10. S. Uemura and K. Torizuka, Appl. Phys. Express **1**, 012007 (2008).
11. H. C. Liang, R. C. C. Chen, Y. J. Huang, K. W. Su, and Y. F. Chen, Opt. Express **16**, 21149 (2008).
12. Y. F. Chen, H. C. Liang, J. C. Tung, K. W. Su, Y. Y. Zhang, H. J. Zhang, H. H. Yu, and J. Y. Wang, Opt. Lett. **37**, 461 (2012).
13. H. C. Liang, Y. J. Huang, W. C. Huang, K. W. Su, and Y. F. Chen, Opt. Lett. **35**, 4 (2010).
14. Y. F. Chen, Y. C. Lee, H. C. Liang, K. Y. Lin, K. W. Su, and K. F. Huang, Opt. Lett. **36**, 4581 (2011).
15. J. Chilla, Q.-Z. Shu, H. Zhou, E. Weiss, M. Reed, and L. Spinelli, Proc. SPIE **6451**, 645109 (2007).
16. D. H. Auston, IEEE J. Quantum Electron. **4**, 420 (1968).
17. P. L. Smith, Proc. IEEE **58**, 1342 (1970).
18. J. L. A. Chilla, H. Zhou, E. Weiss, A. L. Caprara, Q. Shou, S. V. Govorkov, M. K. Reed, and L. Spinelli, Proc. SPIE **5740**, 41 (2005).
19. A. E. Siegman, *Lasers* (University Science Books, 1986), p. 1041.